

# Spatiotemporal chaos and two-dimensional dissipative rogue waves in Lugiato-Lefever model<sup>\*</sup>

Krassimir Panajotov<sup>1,2,a</sup>, Marcel G. Clerc<sup>3</sup>, and Mustapha Tlidi<sup>4</sup>

<sup>1</sup> Department of Applied Physics and Photonics (IR-TONA), Vrije Universiteit Brussels, Pleinlaan 2, 1050 Brussels, Belgium

<sup>2</sup> Institute of Solid State Physics, 72 Tzarigradsko Chaussee Blvd., 1784 Sofia, Bulgaria

<sup>3</sup> Departamento de Física, FCFM, Universidad de Chile, Casilla 487-3, Santiago, Chile

<sup>4</sup> Faculté des Sciences, Optique Nonlinéaire Théorique, Université Libre de Bruxelles (U.L.B.), C.P. 231, Campus Plaine, 1050 Bruxelles, Belgium

Received 31 January 2017 / Received in final form 6 April 2017

Published online 4 July 2017 – © EDP Sciences, Società Italiana di Fisica, Springer-Verlag 2017

**Abstract.** Driven nonlinear optical cavities can exhibit complex spatiotemporal dynamics. We consider the paradigmatic Lugiato-Lefever model describing driven nonlinear optical resonator. This model is one of the most-studied nonlinear equations in optics. It describes a large spectrum of nonlinear phenomena from bistability, to periodic patterns, localized structures, self-pulsating localized structures and to a complex spatiotemporal behavior. The model is considered also as prototype model to describe several optical nonlinear devices such as Kerr media, liquid crystals, left handed materials, nonlinear fiber cavity, and frequency comb generation. We focus our analysis on a spatiotemporal chaotic dynamics in one-dimension. We identify a route to spatiotemporal chaos through an extended quasiperiodicity. We have estimated the Kaplan-Yorke dimension that provides a measure of the strange attractor complexity. Likewise, we show that the Lugiato-Lefever equation supports rogue waves in two-dimensional settings. We characterize rogue-wave formation by computing the probability distribution of the pulse height.

## 1 Introduction

This paper is devoted to the analysis of complex phenomena in the pioneering model proposed by Luigi Lugiato and René Lefever in 1987 [1]. The paradigmatic Lugiato-Lefever equation (LLE) has led to a rich literature that analyses mathematical, computational and experimental aspects of the coupling between nonlinearity, transport process such as diffraction or dispersion, and dissipation. This work also paves a way towards possible applications in encoding/storing information in all optical devices and all-optical memories in fiber based devices.

Recently, complex spatiotemporal dynamics have been a subject of experimental investigations in frequency comb generation [2] and in all fiber cavities with a Kerr-type media [3]. Both systems are well described by the LLE. In most of these studies, complex phenomena are characterized by Fourier spectra, wave vector distributions, filtered spatiotemporal diagrams, power spectra, length distributions, Poincaré maps and number of defects as a function of the parameters. However, these tools are not adequate to characterize for instance spatiotemporal chaos. A rigorous

tools have been proposed in the literature to characterize the spatiotemporal chaos by using Lyapunov exponents or Lyapunov spectrum [4–6]. Lyapunov exponents characterize the exponential sensitivity to initial conditions. When the largest Lyapunov exponent is positive, the complex behavior is chaotic. Furthermore, the spatiotemporal chaos is characterized by a continuous set of positive exponents that constitute the Lyapunov spectrum.

Another line of research is devoted to studying complex phenomena often called rogue waves or extreme events. Rogue waves (RWs) are rare pulses of amplitude much exceeding the average one and they belong to extreme events field of research. They are characterized by a long tail in the probability distribution of pulse amplitude. The formation of RW in optics has been the subject of intense research since the pioneering work by Solli et al. [7] (see the latest overviews on this issue [8–11]). Evidence of rogue waves formation in the framework of LLE have recently been provided in one dimensional setting in both the absence [12] and presence of time-delayed feedback [11].

The goal of this paper is twofold, first, to show that the model LLE supports 2D dissipative rogue waves and second, to identify a new route towards spatiotemporal chaos via extended quasiperiodicity. The term dissipative rogue waves have been introduced by Akhmediev in the context of one-dimensional passively mode-locked lasers [13].

<sup>\*</sup> Contribution to the Topical Issue “Theory and Applications of the Lugiato-Lefever Equation”, edited by Yanne K. Chembo, Damia Gomila, Mustapha Tlidi, Curtis R. Menyuk.

<sup>a</sup> e-mail: kpanajot@b-phot.org

They have been generated in the LLE [14] and in reaction diffusion systems [15]. Here, we show that 2D rogue waves can be generated without any optical feedback and we characterize them by estimating the probability distribution of the pulse height. This distribution possesses a long tail that is considered as the main signature of rogue wave formation. In last part of the manuscript, we show a new route towards spatiotemporal chaos. We characterize this complex regime in one dimensional settings by computing the Lyapunov spectrum.

The paper is organized as follows. In Section 2, we introduce the diffractive and dispersive LLE. The characterization of the spatiotemporal chaos in term of the Lyapunov spectrum is presented in Section 3. The two-dimensional rogue waves are discussed in Section 4. We conclude in Section 5.

## 2 Dispersive and/or diffractive Lugiato-Lefever equation

In their seminal paper [1], Luigi Lugiato and René Lefever, derived a simple and at the same time a very rich model that undergoes a large spectrum of dynamical behaviors often called the LL model. They have considered a one-dimensional nonlinear optical cavity filled with a Kerr medium and driven coherently by an injected signal [1]. More importantly, they established a link between the well know Turing-Prigogine instability in the context of chemical reaction-diffusion systems and the optical spatial instability [1]. Contrarily to the Rayleigh-Bénard instability [16] where the characteristic wavelength of the spatial periodic structures is determined by the geometry, the Turing-Prigogine instability [17,18] possesses a wavelength that is intrinsic to the dynamics of the system. In this case, the wavelength is solely determined by the dynamical parameters and not by the external effects or physical geometrical boundaries. The formation of spatial structures is attributed to the balance between a nonlinear process such as chemical reaction or light matter interaction that tends to amplify inherent spatial fluctuations and a transport process such as diffusion or diffraction that tends on the contrary to restore uniformity. In addition, when the system operates far from equilibrium, dissipation plays an important role in the stabilization of the spatial structures (hence the name dissipative structures [18,19]).

The LL model has been derived for various systems such as all fiber cavity [20], whispering gallery-mode resonators or Kerr frequency-comb generation [12]. In these two systems the diffraction term modeled by the Laplace operator is replaced by chromatic dispersion. The LL model has also been derived for a cavity filled with left-handed material [21–23] or a liquid crystal operating in a self-imaging configuration [24]. In these two systems diffraction coefficient is negative.

The LLE model is valid under the following approximations: the cavity possesses a high Fresnel number, external power can be coupled into the cavity only if the system is close to resonance. This implies that both the linear

cavity detuning and the nonlinear cavity phase shift must be much smaller than unity. In addition, we assume that the cavity is much shorter than the diffraction, dispersion and nonlinearity spatial scales. Furthermore, a single longitudinal mode operation is assumed. In its general form the LLE reads [25,26]

$$\frac{\partial E}{\partial t} = i \left( a \nabla_{\perp}^2 + \beta \frac{\partial^2}{\partial \tau^2} \right) E - (1 + i\theta)E + i|E|^2E + E_i. \quad (1)$$

Here  $E(x, y, t, \tau)$  is the normalized slowly varying envelope of the electric field that circulates within the cavity and  $E_i$  is the amplitude of the injected field which is real and positive in order to fix the origin of the phase. The time variable  $t$  corresponds to the slow evolution of  $E$  over successive round-trips.  $\tau$  accounts for the fast dynamics that describes how the electric field envelope changes along the fiber. The parameter  $\delta$  is the cavity detuning with respect to the injected field.  $\beta$  is the chromatic dispersion coefficient that can be either positive or negative depending whether the dispersion is anomalous or direct, respectively. The diffraction process acting in the transverse plane  $(x, y)$  is modeled by the Laplace operator  $\nabla_{\perp}^2 = \partial^2/\partial x^2 + \partial^2/\partial y^2$ . When the chromatic dispersion is neglected, i.e.,  $\beta = 0$ , it has been shown that the coupling between diffraction and nonlinearity may lead to appearance of stable periodic patterns such as hexagons that emerge from a Turing-Prigogine instability [27]. Indeed, a pattern selection and relative stability analysis in two-dimensional settings show that only hexagonal structures are stable over other periodic patterns [28,29]. When diffraction is neglected, e.g., the intracavity field is spatially stabilized by using guided-wave structures, i.e.,  $a = 0$ , theoretical studies indicate that the coupling between dispersion and Kerr nonlinearity may be the source of a temporal modulational instability leading to the appearance of a periodic train of pulses [20]. When however, the dispersion and the diffraction have a comparable influence, nonlinear analysis of the model equation (1) have revealed the occurrence of a variety of three-dimensional structures in the amplitude of the cavity field among which the body-centered cubic (bcc) lattice structure in the  $(x, y, \tau)$  space plays a dominant role [25,30].

Beside period distribution of light inside the cavity, equation (1) supports localized structures often called cavity solitons in one and in two-dimensional settings [31] when the Turing-Prigogine instability appears sub-critically, i.e.,  $\theta > 41/30$ . In regime devoid of Turing-Prigogine instability, localized structures have been found experimentally and theoretically when the homogeneous steady states are bistable, i.e.,  $\theta > \sqrt{3}$  and when the injected field is inhomogeneous [24].

## 3 Spatiotemporal chaos in LLE

In this section, we characterize a new route towards a spatiotemporal chaos in one dimensional LLE via extended quasiperiodicity. Recently a characterization of the spatiotemporal chaos in LLE has been performed using

a rigorous tool of dynamical system theory based on the Lyapunov spectra [32]. In this work, the destabilization of an oscillatory localized state through radiation of counter propagative fronts between the HSS and the spatiotemporal chaos has been established.

Let us consider a one-dimensional diffractive LLE where  $\nabla_{\perp}^2 = \partial^2/\partial x^2$  by using a waveguide along the  $y$  transverse direction or a dispersive LLE with  $a = 0$  and  $\beta \neq 0$ . The homogeneous steady state (HSS) solutions  $I_S = |E_S|^2$  of equation (1) are given by  $I_i = I_S [1^2 + (I_S - \theta)^2]$  with  $I_i \equiv E_i^2$ . The saddle-node (fold) bifurcation on the HSS  $dI_i/dI_S = 0$  is given by  $I_S^{SN_{h1,2}} = 2\theta/3 \pm \sqrt{\theta^2 - 3}/3$  and therefore,  $I_S$  as a function of  $I_i$  is either monostable for  $\theta \leq \sqrt{3}$  or bistable for  $\theta > \sqrt{3}$  [1]. The linear stability of the HSS results in the quadratic equation for the eigenvalue  $\lambda$ :  $\lambda^2 + 2\lambda + 1 + (\theta - 2I_S + k_{\perp}^2)^2 - I_S^2 = 0$  with  $k_{\perp}$  being the transverse wavenumber. When the eigenvalues are purely real and one of them changes sign from negative to positive, this unstable eigenvalue could correspond either to zero,  $k_{\perp}^2 = 0$ , or to nonzero wavenumber,  $k_{\perp}^2 > 0$ . In the first case, we have saddle-node bifurcations, which correspond to the turning points of the bistable curve and imply that the part of this curve having negative slope is always unstable. The second case indicates the onset of Turing-Prigogine-like instability giving rise to a patterned state. For  $\lambda = 0$  we obtain  $k_{\perp}^2 = -\theta + 2I_S \pm \sqrt{I_S^2 - 1}$  and the existence of real solutions for the wavevector  $k_{\perp}$  indicates the presence of Turing-Prigogine instability. In the limit when marginally stable eigenvalues of the Turing-Prigogine instability tend to zero,  $k_{\perp}^2 \rightarrow 0$  we recover the conditions of the saddle-node bifurcations, i.e.  $I_S^{T(k^2=0)} = I_S^{SN_{h1,2}}$ . We fix the detuning parameter to  $\theta = 2$  for the rest of the paper, i.e. the lower HSS is stable while the upper HSS is totally unstable with respect to Turing-Prigogine instability. Indeed, this can be seen from Figure 1: (a) presents the HSS  $I_S$  as a function of the input intensity and (b) presents the marginal stability curve.

We now consider bifurcation scenario of a localized structure in LLE as a function of the injection field  $E_i = 1.3$ . For small values of injection ( $E_i = 1.3$ ), localized structures are stable. They are similar to the ones that have been predicted in [31]. When increasing the injected field amplitude, transition to a self-organized structure appears at  $t \approx 1200$  and  $E_i \approx 1.42$  as shown in the space-time map of Figure 2a. This map shows the evolution of the intracavity field intensity  $|E|^2(x, t)$  obtained from numerical simulations of the LLE by changing  $E_i$  with a step of 0.02 at each 200 time units. All numerical simulations are obtained by using periodic boundary conditions. The numerical integration is based on Runge-Kutta method combined with a spectral method (pseudo spectral algorithm). At a time of  $t \approx 5700$  the periodic structure becomes unstable and each peak starts to oscillate harmonically – see the time trace and the corresponding power spectrum for the first peak in Figures 2c1 and 2c2, respectively. These figures clearly reveal that the pattern maximum experience period one oscillating dy-

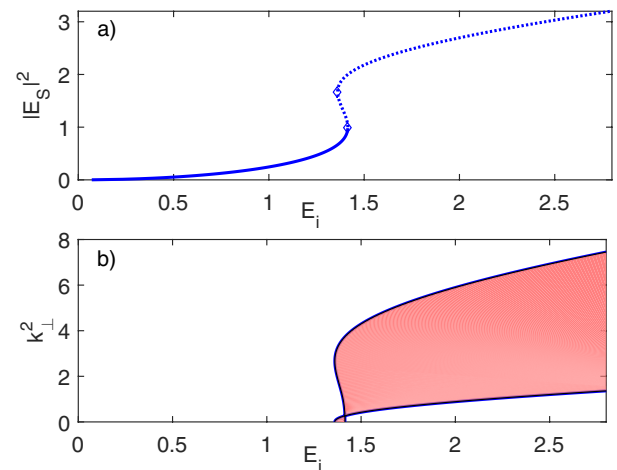


**Fig. 1.** Linear stability analysis of the Lugiato-Lefever model equation (1). (a) Steady-state curves of the homogeneous solution  $I_S$  as a function of the injected field  $E_i$ . Plane-wave stable (unstable) branch is shown with solid (dotted) line and saddle-node bifurcation by diamond symbols. (b) Wavevector square  $k_{\perp}^2$  as a function of the injected field  $E_i$  (red shaded area encompasses all unstable wavevectors). The detuning parameter is  $\theta = 2$ .

namics, i.e. the first temporal instability encountered is an Andronov-Hopf bifurcation with a frequency  $f_1$ . During these oscillations, the neighboring maxima in the pattern oscillate in antiphase; i.e., when one is increasing the neighboring ones are decreasing and vice versa. Increasing further  $E_i$ , the oscillating pattern undergoes a Torus bifurcation with a new, smaller frequency  $f_2$  appearing as shown in Figures 2d1 and 2d2 for a time trace and power spectrum of the third peak. Increasing further  $E_i$ , the system follows an extended quasiperiodic route to chaos with a similar time dependence for each well separated peak of the oscillating pattern – see Figures 2e1 and 2e2 for the time trace and the power spectrum of the fifth peak. For still stronger injection field, the neighboring pattern peaks start to interact strongly with some of them disappearing and reappearing as shown in the bottom regions of Figure 2a. Similar route has been identified from hexagonal patterns in LLE [33] and in non-variational Swift-Hohenberg equation [34]. Note however that in the case of a complex Ginzburg-Landau equation the route to chaos depends on the way of crossing the boundary of the region of chaos [35]. In the case of LLE, by varying the injected field intensity, the route to spatiotemporal chaos depends on the detuning parameter. Two routes have been identified either through period doubling [36] or through extended quasiperiodicity. The route to the chaos of spatially localized light structures through period doubling has been reported for a laser with saturable absorber and delay feedback [37].

In Figure 2b the simulation starts from the high intensity regime ( $E_i = 3.3$ ) and the injected field amplitude  $E_i$  is reduced with a step of 0.02 at each 200 time units. First, the system develops a complex behavior. By reducing the injected field amplitude, a transition from the complex

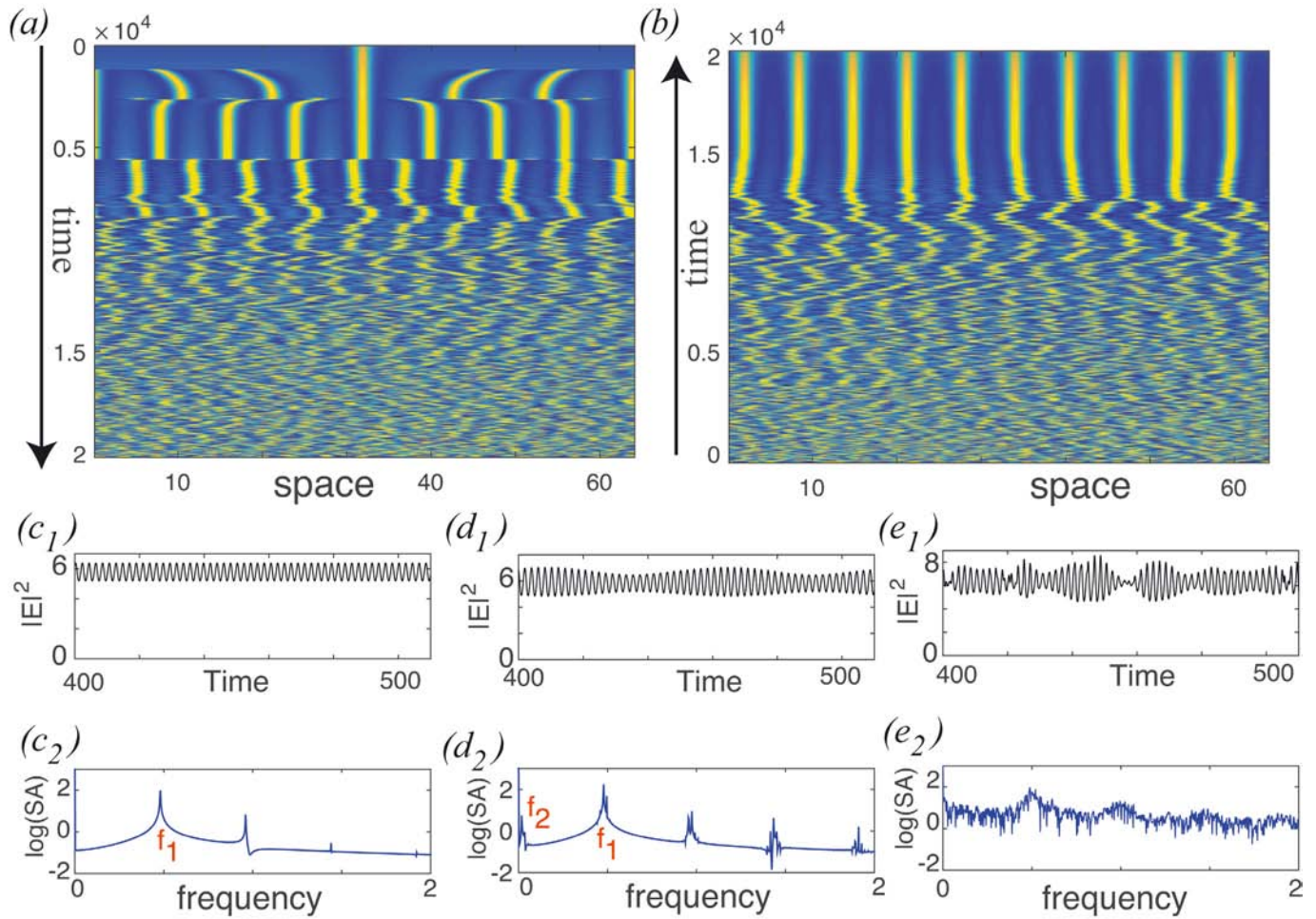


**Fig. 2.** Space-time maps showing the evolution of  $|E|^2(x, t)$  in the LLE when changing  $E_i$  with a step of 0.02 at each 200 time units. Cavity detuning is  $\theta = 2$ . (a)  $E_i$  is increased from 1.3 to 3.3. (b)  $E_i$  is decreased from 3.3 to 1.3. (c1), (d1) and (e1) show time traces for an isolated peak from the periodic pattern for  $E_i = 1.85$ ,  $E_i = 1.9$  and  $E_i = 2.1$ , respectively. (c2), (d2) and (e2) show the corresponding power spectra.

spatiotemporal behavior to a periodic pattern appears. This transition is subcritical and a hysteresis exists as evidenced by comparing Figures 2a and 2b. Interesting switchings between patterns of different wavelength can be seen in Figure 2a for  $t \approx 2700$  and 5600. Such transitions have been discussed in details in this issue by Périnet et al. This change of the wavelength is associated with an Eckhaus instability. In addition, as can be seen by comparing the forward and backward scans in Figures 2a and 2b, the system undergoes a multistable behavior between patterns of a different wavelength.

The characterization of the complex spatiotemporal behavior described above can be achieved by estimating Lyapunov exponents. These exponents provide information about the sensitivity of the LLE to the initial conditions. The Lyapunov exponents are labeled by  $\{\lambda_i\}$ , where  $i = 0, 1, \dots, N$  with  $N$  being the grid number and  $\lambda_p \leq \lambda_q$  ( $p \geq q$ ). The Lyapunov exponent  $\lambda_i$  plotted as a function of  $i$  constitutes the Lyapunov spectrum – see Figure 3a. This spectrum has a continuous set of positive values and therefore we can conclude that the complex spatiotem-

poral behavior described in Figure 1 has a spatiotemporal chaotic nature. In addition, we compute the Kaplan-Yorke dimension ( $D_{YK}$ ) defined by [38]

$$D_{KY} \equiv p + \frac{\sum_{i=0}^p \lambda_i}{\lambda_{p+1}}, \quad (2)$$

where  $p$  is the largest integer that satisfies  $\sum_{i=0}^p \lambda_i > 0$ . The Yorke-Kaplan dimension is an extensive quantity which increases with the system size [4]. In addition, the Kaplan-Yorke dimension provides a measure of the strange attractor complexity. To check the convergence of the numerical method used to establish the Lyapunov spectra, we plot Lyapunov exponents as a function of the integration time as shown in Figure 3b. Finally, the Kaplan-Yorke dimension is plotted as a function of the integration time in Figure 3c to show that it converges towards a value  $D_{YK} = 85$ .

Figure 4 shows the dependence of the largest Lyapunov exponent  $\lambda_0$  (on the left axis) and of the Kaplan-Yorke dimension  $D_{KY}$  (right axis) on the strength of the injection

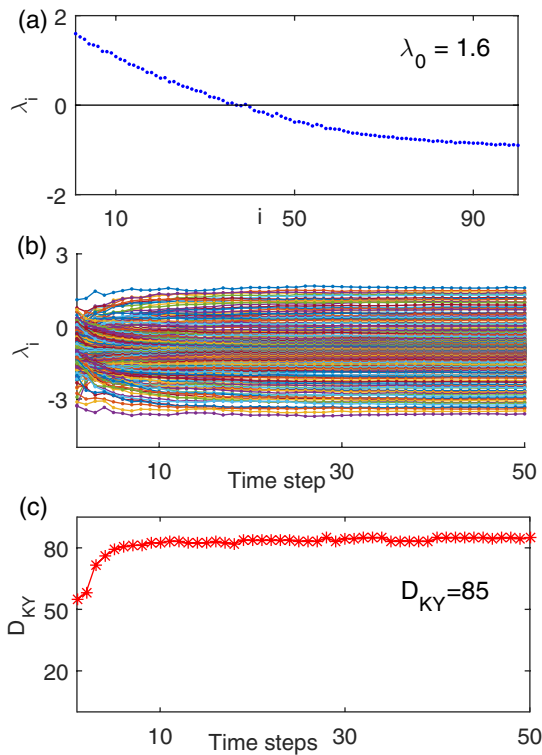


**Fig. 3.** LL model with  $\theta = 2$ ,  $E_i = 5$ . (a) Spectrum of Lyapunov exponents; (b) Lyapunov exponents versus time and (c) Kaplan-Yorke dimension  $D_{KY}$  versus time.

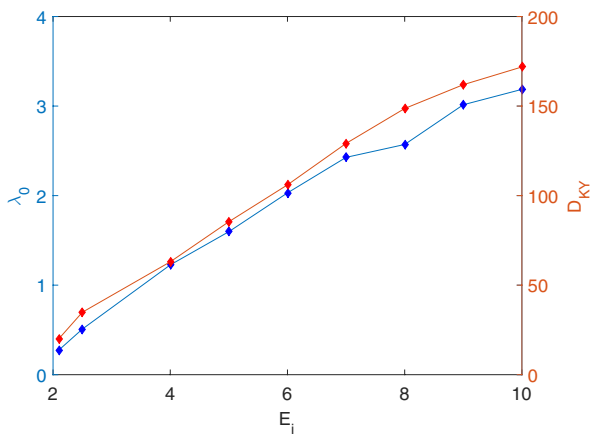


**Fig. 4.** LL model with  $\theta = 2$ . Dependence of the largest Lyapunov exponent  $\lambda_0$  (left axis) and Kaplan-Yorke dimension  $D_{KY}$  (right axis) on the strength of the injection field  $E_i$ .

field  $E_i$ . While the largest Lyapunov exponent indeed increases almost linearly from 0.27 to 3.19, the tremendous increase of Kaplan-Yorke dimension  $D_{KY}$  from about 20 to 170 is mainly due to the development of spatiotemporal chaos with many more positive exponents appearing in the Lyapunov spectrum as  $E_i$  increases.

The above analysis allows us to infer that the spatiotemporal complex behavior reported in the LLE and

describes by Figure 2 belong to a spatiotemporal chaos and it is not a low dimensional chaos or turbulence. In the case of spatiotemporal chaos, the Lyapunov spectrum has a continuous set of positive values as shown in Figure 3b. This is consistent with the definition proposed in [5,6]. In the case of a low dimensional chaos, the Lyapunov spectrum has a discrete set of a few positive values. On the other hand, the turbulence or weak turbulence are characterized by a power law cascade [39]. The power spectrum in the chaotic regime is characterized by displaying an exponential law [40]. On the basis of the Lyapunov and power spectrum, we cannot conclude that the system develops a turbulence. A classification of spatiotemporal complex behaviors can be found in [4–6,34,41,42].

### 4 Rogue waves in two-dimensional Lugiato-Lefever model

The 2007 experimental demonstration of rogue waves in fiber optics has motivated several groups to investigate this intriguing phenomenon [7]. Rogue waves correspond to large intensity pulses in the time domain of resonant fiber cavity. RW formation is also a well documented issue in oceans [43]. Among various mechanisms that have been proposed to be responsible for the generation of rogue waves, the modulational instability mechanism together with pulse collisions remain the main ingredient for the creation of rogue waves as shown by Peregrine [43]. The long tail probability distribution of the wave amplitude is the fundamental characteristics accounting for the generation of rogue waves. In addition, Peregrine solitons are considered as a prototype of rogue waves. Experimental confirmation of Peregrine solitons has been demonstrated in optical fiber [44,45] and in water wave tank [46,47] systems. Small amplitude pulses may grow to large amplitudes if their frequencies belong to a band of unstable mode with a positive gain. Nonlinear interaction between unstable frequencies may lead to a complex wave dynamics. Analytical study of the nonlinear interaction between two frequency solution of the nonlinear Schrodinger equation in the form of the Akhmediev breathers has been reported in [48].

Most of the above mentioned studies have been conducted in one-dimensional systems and in the framework of the Schrodinger nonlinear equation. However, when considering two-dimensional transverse problem, the nonlinear Schrodinger equation is not sufficient to describe rogue waves due to collapse dynamics. Moreover, systems modeled by the LLE are dissipative and operate far from equilibrium regime. In this case, stable two dimensional patterns are possible in the LLE [27]. Patten selection analysis demonstrate that only hexagons are stable over other two-dimensional patterns such as stripes, rhomboids or honeycomb [29]. Two-dimensional spatial confinement of light in the transverse section of the cavity in the form of localized stationary pulses have been theoretically predicted for LLE [31] and experimentally proved in [49]. Several studies have been devoted to studying localized structures often called cavity solitons in the transverse section

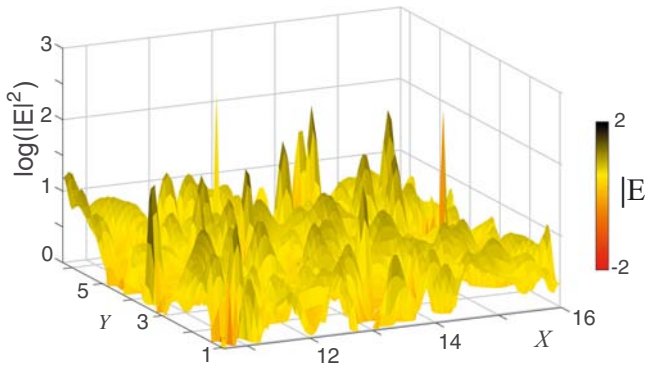


**Fig. 5.** A snapshot of the optical intensity in logarithmic scale for the two-dimensional Lugiato-Lefever model with an extreme event captured. The parameters are  $\theta = 2$  and  $E_i = 5$ .

of spatially extended systems (see recent overviews on this issue [26,50–55]). The interaction of well-separated localized structures has been also investigated [56]. Localized structures can exhibit a self-pulsating instability and spatiotemporal complex phenomena [57,58].

We fix the detuning parameter in the LLE and only vary the strength of the injected field. A single or multi-peak stationary localized structures are formed. They can be either isolated or randomly distributed in the transverse plane peaks appearing in a cluster [31]. When further increasing the injection field  $E_i$ , very high amplitude pulses appear in the region of well developed spatial-temporal chaos (see the snapshot of the optical intensity shown in Fig. 5 for  $\theta = 2$  and  $E_i = 5$ ). A statistical analysis, shown in Figure 6, shows that there is a considerable number of events with spatiotemporal maxima of intracavity intensity more than twice the significant wave height (SWH) and even events with amplitude as high as 6 times the SWH. This figure shows a non Gaussian statistics of the wave intensity, with a long tail of the probability distribution typical for rogue wave formation. We infer that the large intensity pulses generated in Figure 5 belong to the class of rogue waves or extreme events. We would like to emphasize that rogue waves are only formed in the LL model when the spatiotemporal chaos is well developed, i.e. when the neighboring pulses in the oscillating pattern are interacting strongly. For example, Figure 7 displays the statistics of pulse heights in the quasiperiodic and chaotic regimes discussed in the previous section for the 1D LL model. Even when the pulse peaks clearly display chaotic dynamics as in the case of  $E_i = 2.1$  (Fig. 2e), no rogue wave are formed in the system, that is, the tail of the pulse height distribution stays well below  $2 \times$  SWH line. Recently, it has been demonstrated both experimentally and theoretically that intermittency plays a key role for the rogue waves formation in spatially extended microcavity laser with saturable absorber [41,42]. More recently, two-dimensional dissipative rogue waves have been reported in the framework of the LL model and in the laser with saturable absorber with delay feedback [14]. After submission of the present manuscript, a paper by

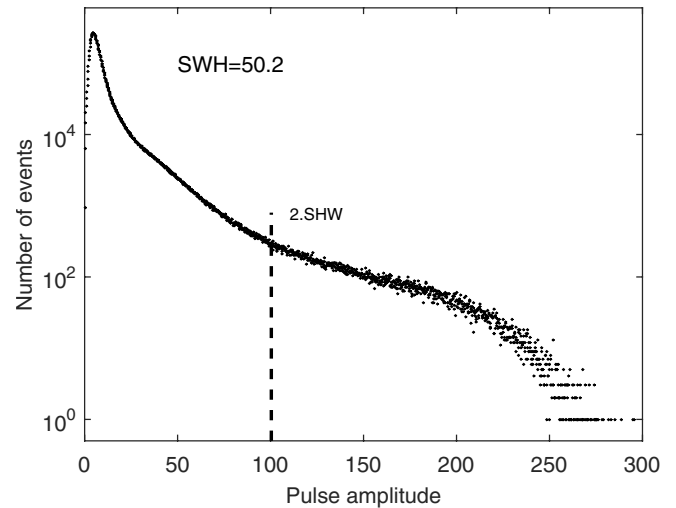


**Fig. 6.** Number of events as a function of the intensity of the pulses in semi-logarithmic scale. LL model parameters are  $\theta = 2$  and  $E_i = 5$ . The SWH denotes the significant wave height. The dashed line indicates  $2 \times$  SWH.

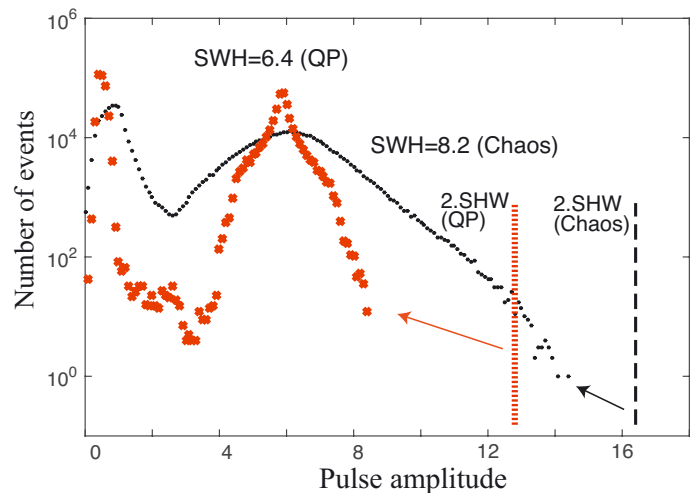


**Fig. 7.** Number of events as a function of the intensity of the pulses in semi-logarithmic scale. LL model in 1D settings with  $\theta = 2$  and  $E_i = 1.9$  (crosses, QP regime) and  $E_i = 2.1$  (circles, chaotic regime). The SWH denotes the significant wave height and the dashed lines indicate  $2 \times$  SWH.

Rimoldi et al. [59] appeared which describes a similar two-dimensional rogue waves for a laser with a saturable absorber without delay feedback.

After reaching a maximum, both the proportion of EEs and the kurtosis of the pulse height probability distribution start to decrease as a function of laser injection current  $\mu$  that drives the system into spatiotemporal chaos, i.e. the Kaplan-Yorke dimension increases with  $\mu$ . It is interesting to check if such a behavior is also observed in the LL model. We have carried out simulations for increasing injection field for the 2D LL model and we have observed different tendency: while the kurtosis indeed decreases with  $E_i$ , the number of EE after an initial sharp decrease begins to gently increase, see Figure 8. Indeed,

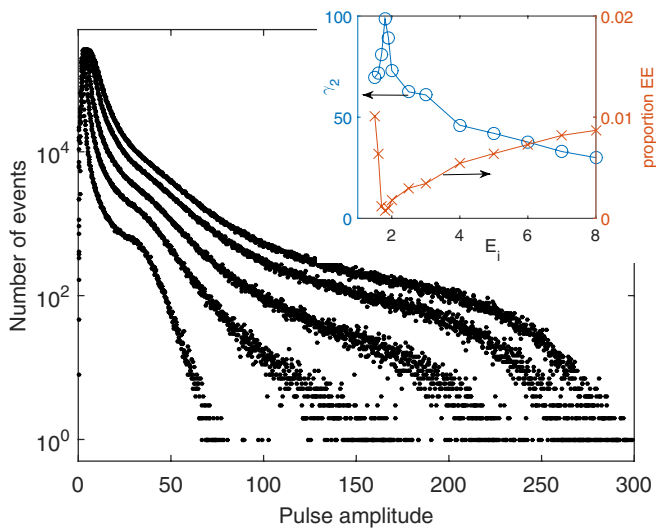


**Fig. 8.** Same as Figure 6 but for different injection field:  $E_i = 1.5, 2, 35$  and  $7$  (distribution curves broaden as  $E_i$  is increased). The inset shows the dependence of Kurtosis (left axis) and the proportion of EE (right axis) as a function of injection field  $E_i$ .

while the kurtosis is an indicative of the deviation of the statistical distribution from Gaussian, the proportion of the EE is an indicative of only the very far tail of the distribution with very large amplitude events (if existing). Therefore, kurtosis and EE proportion are different indicators that can, in principle, behave differently. Additional work is in progress to elucidate the differences in this respect between the LLE and the laser with saturable absorber systems [41,42].

## 5 Conclusions

In this paper, we have investigated the spatiotemporal complex behavior of the one and two-dimensional Lugiato-Lefever equation. A rigorous tool of dynamical system theory, such as Lyapunov spectra, have been used. We have quantitatively shown that the complex behavior observed experimentally in frequency comb generation [2] and in all fiber cavities with a Kerr-type media [3] belong to the spatiotemporal chaos. The Kaplan-Yorke dimension associated with spatiotemporal chaos has been estimated. We have identified a route to spatiotemporal chaos from a periodic structure through an extended quasiperiodicity. Finally, we have identified different operating regimes, in particular, the coexistence between spatiotemporal chaos and the self-organized periodic structure. In the last part of the paper, we have shown that two-dimensional dissipative rogue waves are possible in the LLE. We have characterized this behavior by performing a statistical analysis showing a non-Gaussian profile of the probability distribution with a long tail and pulse intensity height well beyond two times the significant wave height.

M.G.C. thanks for the financial support of FONDECYT Project 1150507. M.G.C., M.T. and K.P. thank the Interuniversity Attraction Poles program of the Belgian Science Policy Office under the grant IAPP7-35. M.T. received support from the Fonds National de la Recherche Scientifique (Belgium). K.P. acknowledges the Methusalem foundation for financial support.

## Author contribution statement

All the authors contributed equally.

## References

1. L.A. Lugiato, R. Lefever, Phys. Rev. Lett. **58**, 2209 (1987)
2. Y.K. Chembo, I.S. Grudinin, N. Yu, Phys. Rev. A **92**, 043818 (2015)
3. M. Anderson, F. Leo, S. Coen, M. Erkintalo, S.G. Murdoch, Optica **3**, 1071 (2016)
4. D. Ruelle, Commun. Math. Phys. **87**, 287 (1982)
5. P. Manneville, *Dissipative Structures and Weak Turbulence* (Academic Press, San Diego, 1990)
6. A. Pikovsky, A. Politi, *Lyapunov Exponents: A Tool to Explore Complex Dynamics* (Cambridge University Press, 2016)
7. D.R. Solli, C. Koonath, B. Jalali, Nature **450**, 1054 (2007)
8. N. Akhmediev, J.M. Dudley, D.R. Solli, S.K. Turitsyn, J. Opt. **15**, 060201 (2013)
9. M. Onorato, S. Residori, U. Bortolozzo, A. Montina, F.T. Arecchi, Phys. Rep. **528**, 47 (2013)
10. M. Dudley, F. Dias, M. Erkintalo, G. Genty, Nat. Photon. **8**, 755 (2014)
11. N. Akhmediev et al., J. Opt. **18**, 063001 (2016)
12. Y.K. Chembo, N. Yu, Phys. Rev. A **82**, 033801 (2010)
13. J.M. Soto-Crespo, Ph. Grelu, N. Akhmediev, Phys. Rev. E **84**, 016604 (2011)
14. M. Tlidi, K. Panajotov, Chaos **27**, 013119 (2017)
15. M. Tlidi, Y. Gandica, G. Sonnino, E. Averlant, K. Panajotov, Entropy **18**, 64 (2016)
16. H. Bénard, Ph.D. thesis, Université de Paris, Thèse de doctorat Sciences physiques, Faculté des sciences de l'Université de Paris, (1901)
17. A.M. Turing, Phil. Trans. R. Soc. Lond. B: Biol. Sci. **237**, 37 (1952)
18. I. Prigogine, R. Lefever, J. Chem. Phys. **48**, 1695 (1968)
19. P. Glansdorff, I. Prigogine, *Thermodynamic Theory of Structure, Stability and Fluctuations* (Wiley Interscience, 1971)
20. M. Haelterman, S. Trillo, S. Wabnitz, Opt. Commun. **91**, 401 (1992)
21. P. Kockaert, P. Tassin, G. Van der Sande, I. Veretennicoff, M. Tlidi, Phys. Rev. A **74**, 033822 (2006)
22. L. Gelens, G. Van der Sande, P. Tassin, M. Tlidi, P. Kockaert, D. Gomila, I. Veretennicoff, J. Danckaert, Phys. Rev. A **75**, 063812 (2007)
23. P. Tassin, G. Van der Sande, N. Veretenov, P. Kockaert, I. Veretennicoff, M. Tlidi, Opt. Express **14**, 9338 (2006)
24. V. Odent, M. Tlidi, M.G. Clerc, P. Glorieux, E. Louvergneaux, Phys. Rev. A **90**, 011806 (2014)

25. M Tlidi, M. Haelterman, P. Mandel, *Quant. Semiclassical Opt.* **10**, (1998)
26. L. Lugiato, F. Prati, M. Brambilla, *Nonlinear Optical Systems* (Cambridge University Press, 2015)
27. W.J. Firth, A.J. Scroggie, G.S. McDonald, L. Lugiato, *Phys. Rev. A* **46**, 3609 (1992)
28. M. Tlidi, Ph.D. thesis, ULB Belgium, unpublished (1995)
29. M. Tlidi, R. Lefever, P. Mandel, *Quant. Semiclassical Opt.* **8**, 931 (1996)
30. M. Tlidi, M. Haelterman, P. Mandel, *Europhys. Lett.* **42**, 505 (1998)
31. A.J. Scroggie, W.J. Firth, G.S. McDonald, M. Tlidi, R. Lefever, L.A. Lugiato, *Chaos Solitons Fract.* **4**, 1323 (1994)
32. Z. Liu, M. Ouali, S. Coulibaly, M.G. Clerc, M. Taki, M. Tlidi, *Opt. Lett.* **24**, 1063 (2017)
33. D. Gomila, P. Colet, *Phys. Rev. A* **68**, 011801 (2003)
34. M.G. Clerc, N. Verschueren, *Phys. Rev. E* **88**, 052916 (2013)
35. N. Akhmediev, J.M. Soto-Crespo, G. Town, *Phys. Rev. E* **63**, 056602 (2001)
36. F. Leo, L. Gelens, P. Emplit, M. Haelterman, S. Coen, *Opt. Express* **21**, 9180 (2013)
37. K. Panajotov, M. Tlidi, *Opt. Lett.* **39**, 4739 (2014)
38. E. Ott, *Chaos in Dynamical Systems*, 2nd edn. (Cambridge University Press, Cambridge, 2002)
39. U. Frisch, *Turbulence: the legacy of AN Kolmogorov* (Cambridge, university press, 1995)
40. A. Coillet, Y.K. Chembo, *Chaos* **24**, 013113 (2014)
41. F. Selmi, S. Coulibaly, Z. Loghmari, I. Sagnes, G. Beaudoin, M.G. Clerc, S. Barbay, *Phys. Rev. Lett.* **116**, 013901 (2016)
42. S. Coulibaly, M.G. Clerc, F. Selmi, S. Barbay, *Phys. Rev. E* **95**, 023816 (2017)
43. D.H. Peregrine, *J. Aust. Math. Soc. Ser. B* **25**, 16 (1983)
44. A. Mussot, E. Louvergneaux, N. Akhmediev, F. Reynaud, L. Delage, M. Taki, *Phys. Rev. Lett.* **101**, 113904 (2008)
45. B. Kibler, J. Fatome, C. Finot, G. Millot, F. Dias, G. Genty, N. Akhmediev, J.M. Dudley, *Nat. Phys.* **6**, 790 (2010)
46. A. Chabchoub, N.P. Hoffmann, N. Akhmediev, *Phys. Rev. Lett.* **106**, 204502 (2011)
47. A. Chabchoub, N. Akhmediev, N.P. Hoffmann, *Phys. Rev. E* **86**, 016311 (2012)
48. N. Akhmediev, J.M. Soto-Crespo, A. Ankiewicz, *Phys. Lett. A* **373**, 2137 (2009)
49. V. Odent, M. Taki, E. Louvergneaux, *New J. Phys.* **13**, 113026 (2011)
50. M. Tlidi, M. Taki, T. Kolokolnikov, *Chaos* **17**, 037101 (2007)
51. N. Akhmediev, A. Ankiewicz (eds.), *Dissipative Solitons: from Optics to Biology and Medicine*, Lecture Notes in Physics (Springer, Heidelberg, 2008), Vol. 751
52. H. Leblond, D. Mihalache, *Phys. Rep.* **523**, 61 (2013)
53. O. Descalzi, M.G. Clerc, S. Residori, G. Assanto, *Localized States in Physics: Solitons and Patterns: Solitons and Patterns* (Springer, 2011)
54. M. Tlidi, K. Staliunas, K. Panajotov, A.G. Vladimirov, M. Clerc, *Phil. Trans. R. Soc. A* **372**, 20140101 (2014)
55. M. Tlidi, M.G. Clerc (eds.), *Nonlinear Dynamics: Materials, Theory and Experiments* (Springer Proceedings in Physics, 2016), Vol. 173
56. D. Turaev, A.G. Vladimirov, S. Zelik, *Phys. Rev. Lett.* **108**, 263906 (2012)
57. W.J. Firth, G.K. Harkness, A. Lord, J.M. McSloy, D. Gomila, P. Colet, *J. Opt. Soc. Am. B* **19**, 747 (2002)
58. P. Parra-Rivas, D. Gomila, M.A. Matas, S. Coen, L. Gelens, *Phys. Rev. A* **89**, 043813 (2014)
59. C. Rimoldi, S. Barland, F. Prati, G. Tissoni, *Phys. Rev. A* **95**, 023841 (2017)
60. K. Panajotov, D. Puzyrev, A.G. Vladimirov, S.V. Gurevich, M. Tlidi, *Phys. Rev. A* **93**, 043835 (2016)